JOURNAL OF PROPULSION AND POWER
Vol. 11, No. 4, July–August 1995

Two-Phase Flows in the Nozzles of Solid Rocket Motors

I. M. Vasenin* and R. K. Narimanov†
Tomsk State University, Tomsk 634050, Russia
and
A. A. Glazunov,‡ N. E. Kuvshinov,§ and V. A. Ivanov§
Research Institute of Applied Mathematics and Mechanics, Tomsk 634050, Russia

Physicomathematical models of multivelocity and multitemperature two-phase flows are suggested. The analyses take into account the particle rotation due to off-center collisions in solid rocket motor (SRM) nozzles and the effects of crossing the trajectories of other particles in the combustion chamber. The rotation of particles is treated by means of quasi-one-dimensional approximation. The effect of the rotation on particle-size distribution and two-phase losses is shown. Three-dimensional two-phase flows in SRM nozzles with rectangular cross sections are considered. The influence of nozzle geometry on the gasdynamic structure of two-phase flow is determined. Axisymmetric calculations are performed for the flows in the combustion chambers and nozzles of SRM. The calculations show the importance of taking into account the intersection of particle trajectories in investigating flows in motors with charges of complex geometry.

Nomenclature

A = number of particle collisions
a = sound velocity
c = specific heat
c_p = specific heat of gas at constant pressure
d = particle diameter
d_{43} = mass mean particle diameter
E = total energy of unit volume
F = cross-sectional area
F_S^α = drag force projection on x axis
$\mathbf{F}_S^\alpha$ = drag force vector of particles
H_0 = total enthalpy
I = moment of inertia of particle
K = coagulation constant
Lp = Laplace number
M = Mach number
M_i = rotational moment of particle
M_0 = rotational moment of a system consisting of two nonrotating liquid particles
m = particle mass
N = number of particle fractions
Nu = Nusselt number
n = number of particles per unit volume
P = pressure
Pr = Prandtl number
Q_{li} = coagulation term
R = gas constant
Re = Reynolds number
r = particle radius
r_{43} = mass mean radius, $d_{43}/2$
T = temperature
t = time
$\mathbf{U}$ = velocity vector
u, v, w = dimensionless velocity components along x, y, and z axes, respectively
We = Weber number
x, y = coordinate axes
z = weight fraction of condensed phase or coordinate axis
ε = capture coefficient
ζ, η, ξ = coordinate axes
η = dynamic viscosity coefficient
κ = adiabate index
λ = thermal conductivity
ξ_p = two-phase loss
ρ = density of two-phase medium
ρ_i = dimensionless "particle-seeded gas" density
σ = surface tension coefficient
ϕ = collision efficiency coefficient
$\varphi_{Ai}, \varphi_{Mi}, \varphi_{Ri}$ = interaction coefficients
Ω = dimensionless rotational moment of particle

Subscripts

a = nozzle exit section
B = particle substance
H = nozzle inlet (head) section
i, j, q, s, l = particle fractions
J = nozzle joint section
k = x_k projection of vector
m = nozzle throat
ref = reference
0 = zero flow velocity
* = critical

Superscripts

α, β = particle flow numbers

Special Signs

∇ = Hamilton gradient operator
$(\cdot)$ = scalar products of vectors

Received Dec. 1, 1993; revision received Feb. 7, 1995; accepted for publication Feb. 7, 1995.

*Professor, Head of Department of Applied Aeromechanics.
†Postgraduate Student, Department of Applied Aeromechanics.
‡Ph.D., Head of Laboratory.
§Ph.D., Senior Researcher.

Introduction

THE investigation of two-phase flows in the nozzles of solid–propellant rocket motors is stimulated by practical problems facing designers in improving available propulsion systems and creating new systems. Essential contributions to the understanding and mathematical description of the extremely complex phenomena arising in the motion of two-

phase flows in nozzles have been made by numerous researchers. Several books and reviews have addressed the different aspects of two-phase flows in nozzles (see Refs. 1–11 and references therein). However, a number of processes that accompany the two-phase flows in nozzles are as yet little understood. Some of these processes are considered in this article.

It is known that the two-phase flow in a nozzle involves a change in size distribution of the liquid particles of metal oxides due to coagulation and breaking. Since the size distribution of the particles and their weight fraction in the flow affect the energy-thrust characteristics of the nozzle appreciably, considerable attention has been directed toward the development and numerical realization of mathematical models describing the two-phase flows in nozzles, taking into account the coagulation and breaking of particles.

In early works,[12–15] the interaction between the particles assumed their total coagulation. This approach resulted in overestimated values of particle size and two-phase losses in specific impulse. The next step in studying the particle interaction came from Alemasov et al.,[1] who, based on physical considerations, introduced a correction factor less than unity for the coagulation constant. Although this slightly reduced the calculated values of the two-phase losses in specific impulse and the mass-averaged particle size, they still exceeded corresponding experimental values. In further investigations, a two-phase flow model taking into account the merging and breaking of particles was employed widely.[3,5,6,16] Some models were proposed for describing the shape and parameters of the fragments resulting from particle breaking.[3,5,6,17]

It should be noted that none of the models describing polydisperse flows, including the merging and breaking of particles, take into account the collision-induced rotation of particles. In fact, in off-center collisions, a system of two nonrotating particles is characterized by a rotational moment. Therefore, the coagulates resulting from the collision always rotate. According to experimental data,[6] particles resulting from collision-induced breaking also rotate.

In the first section of this article, a physicomathematical model of a two-phase flow is suggested, taking into account the rotation of particles. The model is used for the analysis of the influence of particle rotation on the gasdynamic flow pattern and on the energy-thrust characteristics of solid rocket motor (SRM) nozzles.

The necessity of mathematical simulation of two-phase three-dimensional flows in SRM nozzles stems from the fact that in some cases nozzles with square, rectangular, ellipsoid, or combined cross sections are needed. For such nozzle configurations, it is necessary to analyze the influence of nozzle geometry on the flow pattern and thrust characteristics.

A great deal of research has been devoted to the numerical investigation of two-phase three-dimensional flows in SRM nozzles.[4,9,18–25] Early works were concerned with the analysis of the flows in the supersonic zones of the nozzles. Two-phase monodisperse flows in the supersonic zone of elliptic nozzles were studied by Rychkov and Tkachenko.[9,18,21] Three-dimensional flows in movable nozzles have been investigated. The qualitative pattern of the flow as well as the dependencies of some integral characteristics (the loss of specific impulse by particle scattering and precipitation and the deflection coefficient of the thrust vector) on nozzle deflection angle have been shown for different particle sizes and weight fractions of the condensed phase. I-Shih Chang[19] has considered three-dimensional two-phase supersonic flows in nozzles of various configurations. The structure of such flows has been shown to differ essentially from that of gas flows. For the nozzles of the geometry considered, it has been demonstrated that the flow involves a shock wave of complex geometry.

The procedure for calculation of two-phase flows in the subtransonic zone is more complicated.[22,23] The second section of this article reports the results of the study of two-phase flows, taking into account the merging, breaking, and rotation of particles for various rectangular nozzles.

The flow entering a nozzle is formed in the SRM chamber and, hence, the flow parameters are determined by in-chamber processes. The requirements imposed on up-to-date rocket motors determine the variety of the shapes and sizes of SRM charges. The simplest configuration of free volume in the charge is the cylindrical channel. Gas is supplied to the channel from the walls. The flow in such a channel is considered uniform, the velocity and thermal lags being ignored. Some works postulate that the velocities and temperature of all particles of the same size moving through the channel are equal. However, the particles of the same mass fraction may have different parameters due to different prehistories. For example, a particle of a certain mass can enter a given zone moving along the channel without collisions, while other particles of the same mass can enter this zone just after their formation via merging or breaking. The contribution of collisions of particles in their chaotic motion in nozzles has been considered.[6,26] It has been shown that the collision-induced fluctuations of motion enhance the coagulation of particles of similar sizes and increase the loss in specific thrust impulse. For charges of complicated geometry, there is one more reason for the velocity and temperature differences of equal-size particles, the difference in the parameters of particles at the instant of their appearance in the charge channel. A two-phase flow model that allows calculations for crossing paths of particles, as well as examples of its application, are presented in. the third section of this article.

Quasi-One-Dimensional Flow with Coagulation, Breakage, and Rotation of Particles

In off-center collisions, a system consisting of two nonrotating liquid particles possesses the rotational moment

$$M_0 = \frac{m_1 m_2}{m_1 + m_2}[r_{12} \times (U_1 - U_2)] \tag{1}$$

where r_{12} is the characteristic distance between the particles in collision. According to the law of conservation of the momentum, particles resulting from breaking and merging always rotate. Furthermore, secondary particles resulting from collision-induced breaking also rotate.[10] In this case, the rotation is determined by the action of the tangent of the friction component in the "sliding" of particles relative to each other. In the latter case, as a rule, only the largest particle rotates, while small fragments cease to rotate because of the decelerating effect of the crosspieces arising from the destruction of liquid particles.

Particles in the nozzle undergo repeated collisions. This brings up the question: What rotational moment can a particle acquire after a large number of sequential collisions if each collision adds a rotational moment of ΔM_i? The change of rotational moments of particles for a series of collisions was computer-simulated. The calculated particle paths in the plane of moments for random additions of ΔM_i resemble the particle paths characteristic of the Brownian motion.[6] Proceeding from this similarity, the particles with zero initial moments would be expected to "diffuse" in the plane of moments due to collisions. If the rotation decay caused by friction in viscous gas is rather small, repeatedly colliding particles will gather momentum until they are destroyed by centrifugal forces. To take this effect into account in calculating a two-phase flow in a nozzle, one should know the function of particle distribution in the rotational moment. However, the introduction of one more independent variable increases the dimensionality of the calculation domain, which is undesirable from the standpoint of calculation feasibility. Therefore, in addition to the equations describing the two-phase flow (including particle merging and breaking), a simplified equation has been

obtained for the mean value of rotational moment square for particles of each fraction[6]

$$\frac{dM_i^2}{dt} + \frac{2B_iM_i^2}{I_i} = \sum_{j=1}^{i} K_{ij}(M_1^{*2} - M_i^2)n_j + \sum_{j=i}^{N} K_{ij}(1 - \phi_{ij})(M_2^{*2} - M_i^2)n_j \quad (2)$$

where M_1^{*2} and M_2^{*2} are the squares of proper rotational moments of fragments, and B_i is the drag coefficient for the momentum of the force acting as the particles form the gas flow.

In this work, the two-phase flow model was employed in calculating two-phase flows in SRM nozzles. A quasi-one-dimensional nonequilibrium two-phase flow is considered in a SRM nozzle whose cross-sectional area changes as $F(x)$. In terms of a multiple liquid model of a continuum, the problem for a stationary two-phase flow (including merging, breaking, and rotation of particles) has the form[27]

$$F\rho U = G_g = \text{const} \quad (3)$$

$$\frac{d}{dx} F\rho U^2 + F\frac{d}{dx} P = F\sum_{i=1}^{N} \rho_i\varphi_{Ri}(U_i - U) \quad (4)$$

$$\frac{d}{dx} F\rho UH_0 = F\sum_{i=1}^{N} \rho_i[\varphi_{Ai}c_p(T_i - T) + \varphi_{Ri}U_i(U_i - U)] \quad (5)$$

$$P = \rho\frac{\kappa - 1}{\kappa}\left(H_0 - \frac{U^2}{2}\right) \quad (6)$$

$$\frac{d}{dx} F\rho_iU_i = FQ_{1i}, \qquad \frac{d}{dx} Fn_iU_i = FQ_{2i} \quad (7)$$

$$\frac{d}{dx} F\rho_iU_i^2 = F[\rho_i\varphi_{Ri}(U - U_i) + Q_{3i}] \quad (8)$$

$$\frac{d}{dx} F\rho_iU_iE_i = F\{\rho_i[\varphi_{Ai}c_p(T - T_i) + \varphi_{Ri}U_i(U - U_i)] + Q_{4i}\} \quad (9)$$

$$\frac{d}{dx} Fn_iU_iM_i^2 = F(n_i\varphi_{Mi}M_i^2 + Q_{5i}) \quad (10)$$

Here, G_g is the gas flow rate and Q_{li} ($l = 1, \ldots, 5$) are the coagulation terms. The force interaction coefficient φ_{Ri} is determined by Henderson's equation,[28] with the coefficient of thermal interaction φ_{Ai} being borrowed from Ref. 29. The coefficient of rotational interaction between gas and particles, as mentioned earlier,[6] can be defined in the Stokes approximation $\varphi_{Mi} = -30\eta/(\rho_{Bi}r_i^2)$.

Possible fracture of particles due to gas blowing is taken into account (it is assumed that if the Weber criterion exceeds the critical value $We_* = 17$, the particle is broken into two equal pieces). If the normalized rotational momentum

$$\Omega = |M_i|/(r_i^{7/2}\cdot\sqrt{\rho_B\sigma_B}) \quad (11)$$

exceeds $\Omega_* = 6$, the centrifugal forces break the particle into two equal fragments with zero rotational moments.

The interaction of particles was calculated in terms of the continuous approach by the "labeled particles" method[6] (in the literature this method is termed the Lagrangian method). The "monodisperse" and "polydisperse" models of fragments were used.[3,5] Within the framework of the monodisperse model, the coagulation terms are as follows[3,6]:

$$Q_{1i} = n_i\sum_{j=1}^{i} K_{ij}\varepsilon_{ij}\phi_{ij}\rho_j - \rho_i\sum_{j=i}^{N} K_{ij}\varepsilon_{ij}\phi_{ij}n_j \quad (12)$$

$$Q_{2i} = -n_i\sum_{j=i}^{N} K_{ij}\varepsilon_{ij}\phi_{ij}n_j \quad (13)$$

$$Q_{3i} = n_i\sum_{j=1}^{i} K_{ij}\varepsilon_{ij}\rho_j[U_j - (1 - \phi_{ij})U_i] - \rho_i\sum_{j=i}^{N} K_{ij}\varepsilon_{ij}n_j[U_i - (1 - \phi_{ij})U_j] \quad (14)$$

$$Q_{4i} = n_i\sum_{j=1}^{i} K_{ij}\varepsilon_{ij}\rho_j[E_j - (1 - \phi_{ij})E_i] - \rho_i\sum_{j=i}^{N} K_{ij}\varepsilon_{ij}n_j[E_i - (1 - \phi_{ij})E_j] \quad (15)$$

$$Q_{5i} = n_i\sum_{j=1}^{i} K_{ij}\varepsilon_{ij}n_j(M_{1ij}^{*2} - M_i^2) + n_i\sum_{j=i}^{N} K_{ij}\varepsilon_{ij}(1 - \phi_{ij}) \times (M_{2ij}^{*2} - M_i^2)n_j - n_iM_i^2\sum_{j=i}^{N} K_{ij}\varepsilon_{ij}\phi_{ij}n_j \quad (16)$$

Here, $M_{1ij}^{*2} = \alpha_{10}M_{0ij}^2 + \alpha_{11}M_i^2 + \alpha_{12}M_j^2$, $M_{2ij}^{*2} = \alpha_{20}M_{0ij}^2 + \alpha_{21}M_i^2 + \alpha_{22}M_j^2$, and $E_i = c_BT_i + U_i^2/2$. The values of α_{ij} ($i = 1, 2$; $j = 0, 1, 2$) must be set as functions of masses, velocities, and temperatures of colliding particles. The values derived from data obtained by filming collisions are as follows[6]: $\alpha_{10} \approx 0.0578$, $\alpha_{11} \approx 1$, and $\alpha_{12} \approx 0$. Estimations have shown that the values of M_{2ij}^{*2} can be negligible compared to those of M_{1ij}^{*2}.

The polydisperse model implies that target fragments are distributed over all fractions of missile particles in accordance with the mass-normalized distribution function of the ith fragments α_{qij}^5 resulting from the collisions of the particles of r_q and r_j ($r_j > r_q$). The initial velocities and temperatures of the fragments are determined using the experimental constants β, γ in the following relationships[5]:

$$U_{qji} = U_j + \beta(U_q - U_j), \qquad T_{qji} = T_j + \gamma(T_q - T_j), \qquad \beta = 0.08, \quad \gamma = 0.01 \quad (17)$$

In the polydisperse model of fragments, the source terms are as follows[5,9]:

$$Q_{1i} = n_i\sum_{j=1}^{i} K_{ij}\varepsilon_{ij}\phi_{ij}\rho_j - \rho_i\sum_{j=i}^{N} K_{ij}\varepsilon_{ij}n_j + \sum_{j=i}^{N}\sum_{q=1}^{j} K_{qj}\varepsilon_{qj}n_j(1 - \phi_{qj})\alpha_{qji}\rho_q \quad (18)$$

$$Q_{2i} = \frac{n_i}{\rho_i}\left[\sum_{j=i}^{N}\sum_{q=1}^{j} n_jK_{qj}\varepsilon_{qj}(1 - \phi_{qj})\alpha_{qji}\rho_q - \rho_i\sum_{j=i}^{N} K_{ij}\varepsilon_{ij}n_j\right] \quad (19)$$

$$Q_{3i} = n_i\sum_{j=1}^{i} K_{ij}\varepsilon_{ij}\rho_j\{U_j - (1 - \phi_{ij})[U_i + \beta(U_j - U_i)]\} - \rho_iU_i\sum_{j=i}^{N} K_{ij}\varepsilon_{ij}n_j + \sum_{j=i}^{N}\sum_{q=1}^{j} n_jK_{qj}(1 - \phi_{qj})\alpha_{qji} \times [U_j + \beta(U_q - U_j)] \quad (20)$$

$$Q_{4i} = n_i \sum_{j=1}^{i} K_{ij}\varepsilon_{ij}\rho_j \left(\left(c_B T_j + \frac{1}{2} U_j^2\right) - (1 - \phi_{ij})\left\{c_B[T_i + \gamma(T_j - T_i) + \frac{1}{2}[U_i + \beta(U_j - U_i)]^2\right\}\right) - \rho_i \left(c_B T_i + \frac{1}{2} U_i^2\right) \sum_{j=i}^{N} K_{ij}\varepsilon_{ij} n_j + \sum_{j=i}^{N} \sum_{q=1}^{j} \rho_q n_j K_{qj}(1 - \phi_{qj})\alpha_{qji}\left\{c_B[T_j + \gamma(T_q - T_j)] + \frac{1}{2}[U_j + \beta(U_q - U_j)]^2\right\} \quad (21)$$

In terms of this model, taking into account the rotation of particles requires data on the distribution of the square of the rotational moment in fragments. Unfortunately, these data are presently not available. However, the rotational moments of droplets in collisions[6] estimated from experimental results allow the monodisperse equation for the square of the rotational moment to be extended to the case of polydisperse fragments, since in the collision of viscous droplets the momentum of the system almost totally gas into the momentum of the largest fragment.

Equations (18–21) incorporate the capture coefficient ε_{ij}, the collision efficiency factor ϕ_{ij}, and the coagulation constant K_{ij}. The value of ε_{ij} was determined by the empirical dependence obtained by Langmure and Blodgett (see Ref. 3). ϕ_{ij} was set as follows[5]:

$$\phi_{ij} = 1 - 0.246 Re_{Bij}^{0.407} Lp_j^{-0.096} (r_j/r_i)^{-0.278}$$
$$30 < Re_{Bij} < 600, \quad 5 < Lp_j < 3 \cdot 10^5, \quad 1.9 < (r_j/r_i) < 12 \quad (22)$$

Here, $Re_{Bij} = 2|U_i - U_j| r_i \rho_{Bj}/\eta_{Bj}$ is the Reynolds number, and $Lp_j = 2 r_j \sigma_{Bj} \rho_{Bj}/\eta^2_{Bj}$ is the Laplace number.

This dependence disregards the effect of the gas flow on particle collisions. The effect could be taken into account as a correction of the general function[8]

$$\tilde{\phi}_{ij} = \phi_{ij} - \varphi_{ij}$$
$$\varphi_{ij} = \begin{bmatrix} 0.00446 B_{ij}, & B_{ij} \le 40.6 \\ 11.9(B_{ij}/100)^{4.64}, & 40.6 < B_{ij} < 120 \end{bmatrix} \quad (23)$$

where $B_{ij} = Re_{Bij}^{0.285} Lp_j^{0.2} (r_j/r_i)^{0.4} We_j^{0.442}$ and $We_j = 2 r_j \rho (U - U_i)^2/\sigma_{Bj}$ is the Weber number. At $30 < Re_{Bij} < 500$, $8 \le Lp_j \le 10^3$, and $2.5 < (r_j/r_i) < 10$, $We_j < 12.5$.

For the nozzle inlet section, temperature and velocity equilibrium between the gas phase and particles was assumed ($U_i = U$, $T_i = T$). The values of ρ_i and n_i were determined by setting a mean-mass diameter d_{43} and assuming the normal-logarithmic distribution of particles in size or uniform distribution in mass. The squares of the rotational moments of particles at the inlet cross section for all particle fractions were set to be zero.

Numerical calculations were performed for a nozzle consisting of six sections (Fig. 1): 1) an inlet cylindrical section; 2) an initial section specified by an arc of radius r_1; 3) a converging section with a semiangle θ_1; 4), 5) sections represented by arcs of radii r_2 and r_3, respectively; and 6) a diverging section set by a cubic parabola arc with angles θ_2 and θ_3, where θ_2 is the slope of the arc at the point of its joint with a circle of radius r_2, and θ_3 is the arc slope at the nozzle exit section.

The dimensionless data (all linear values are related to r_m where $r_m = 0.0925$ m) for setting the nozzle geometry were as follows: the horizontal coordinate of nozzle inlet section $x_H = -2.0$; the horizontal coordinate of nozzle throat $x_m = 0.0$; the horizontal coordinate of nozzle exit section $x_a = 8.1643$; the inlet section ordinate $r_H = 1.7$; the exit section ordinate $r_a = 4.0$; $r_1 = 1.0$; $r_2 = 1.0$; $r_3 = 0.2$; $\theta_1 = 45$ deg; $\theta_2 = 24$ deg; and $\theta_3 = 7$ deg. The conditions in the combustion chamber and the combustion product characteristics were set as follows: $P_0 = 6$ MN/m^2, $T_0 = 3500$ K, $z = 0.4$, $\kappa = 1.13$, $\eta_0 = 9 \times 10^{-5}$ kg/(m·s), and $Pr = 0.768$.

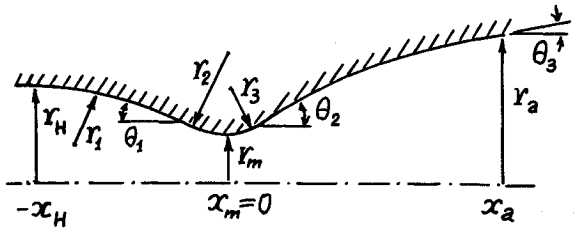

Fig. 1 Nozzle profile.

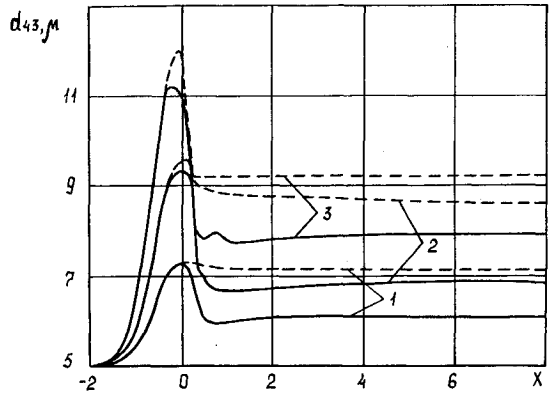

Fig. 2 Change in d_{43} along the nozzle at different weight fractions of the condensed phase: 1) $z = 0.2$, 2) $z = 0.4$, and 3) $z = 0.6$. Solid lines, particles rotate; and dashed lines, rotation is neglected.

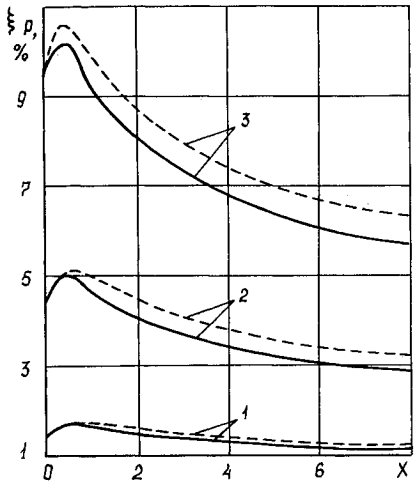

Fig. 3 Change in two-phase flow losses along the nozzle at different weight fractions of the condensed phase: 1) $z = 0.2$, 2) $z = 0.4$, and 3) $z = 0.6$. Solid lines, particles rotate; and dashed lines, rotation is neglected.

It is well-known that the character of the two-phase flow depends to a large extent on the condensed phase fraction by weight. Figures 2 and 3 show changes in the mean mass diameter of particles d_{43} and the two-phase flow loss coefficient $\xi_p(\%)$ along the nozzle for $z = 0.2$, 0.4, and 0.6. The dashed lines show the same dependencies without regard for particle rotation. It can be seen that the effect of particle rotation increases with z. This is illustrated by Fig. 4, which shows the two-phase flow loss at the nozzle exit as a function of z for three different values of throat radius.

The numerical simulation was performed in terms of the monodisperse model of fragments. It is of interest to analyze

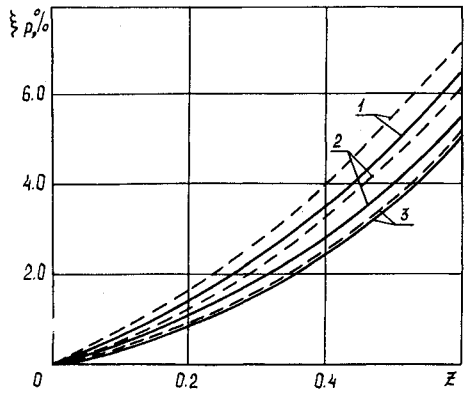

Fig. 4 Two-phase flow losses at the nozzle exit as a function of z at different r_m: 1) $r_m = 0.06$ m, 2) $r_m = 0.0925$ m, and 3) $r_m = 0.125$ m. Solid lines, particles rotate; and dashed lines, rotation is neglected.

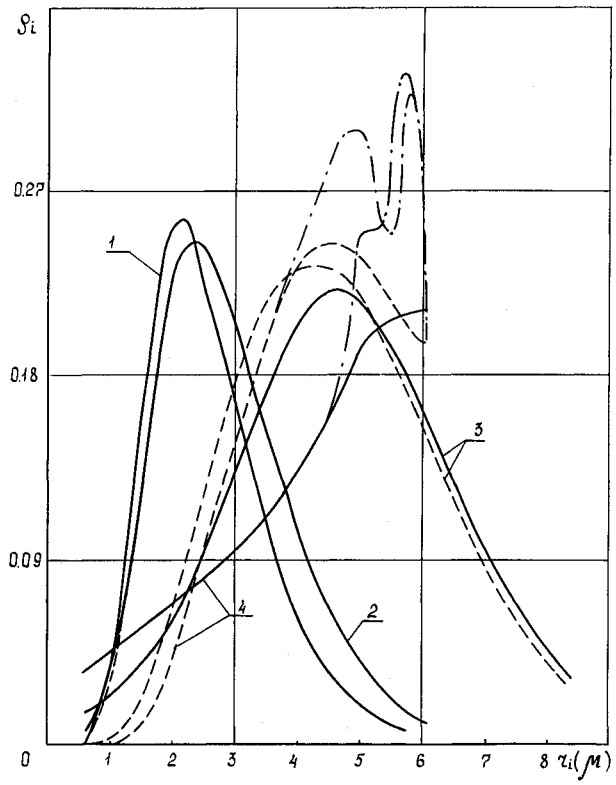

Fig. 5 Distribution of the ρ_i in two fragmentation models at different nozzle sections: 1) $x = -2$, 2) $x = -1.0$, 3) $x = 0.0$, and 4) $x = 8.0$. Solid line, polydisperse model; dashed line, monodisperse model; and dash–dot line, contribution due to the particle breakage caused by the reaching We_* or Ω_*.

the effect of particle rotation in terms of the polydisperse model of fragments. Figure 5 shows the evolution of the dimensionless density of the particle-seeded gas ρ_i, which is equal to the mass of particles of a given size per unit volume, referred to as the density of two-phase medium, for four nozzle sections. Note that the qualitative pattern of the behavior of $\rho_i(x)$ is the same for both models (solid line, polydisperse model; dashed line, monodisperse model). First, due to the prevailing coagulation of particles, $\rho_i(x)$ is shifted to the region of coarse particles, with the portion of intermediate-size particles decreasing. Then, the breakage of large particles becomes dominant and the portion of intermediate-size particles increases. Most importance in this case is the breakage of particles reaching the critical values of We_* or Ω_*. The contribution to ρ_i due to the action of these factors

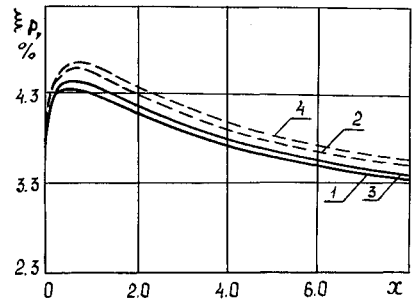

Fig. 6 Change in $\xi_p(\%)$ along the nozzle for different fragmentation models: solid line, polydisperse model; and dashed line, monodisperse model. 1), 2) particles rotate and 3), 4) rotation is neglected.

is shown in the dash–dot lines in Fig. 5. The nonmonotonic behavior of these lines is accounted for by the limited number of calculated fractions of particles.

The magnitude of the two-phase flow loss depends on the behavior of $\rho_i(x)$. The curves for the polydisperse model of fragments are more flat than those for the monodisperse model; this effect is more pronounced for small particles because in the Lagrangian representation the monodisperse model implies the exhaustion of the least particles, while the polydisperse model implies that this fraction is continuously supplied with the fragments of collision-broken particles. As a result (Fig. 6), the monodisperse model (curve 2) of fragments gives an insignificant increase in two-phase flow loss as compared with the more accurate polydisperse model (curve 1). Calculations performed without regard for particle rotation yield a similar result (curve 2 in Fig. 6, with particle rotation taken into account; and curve 4, with particle rotation disregarded).

The calculations by the polydisperse model of fragments are much more time-consuming than the calculations by the monodisperse model. Thus, in predesign calculations the monodisperse model can be employed. However, this model is inapplicable to the three-dimensional case, where the mass and momentum of the particles precipitated along the profile of the designed nozzle should be taken into account. An investigation of two-phase axisymmetric flows in SRM nozzles has been described elsewhere.[30]

Three-Dimensional Two-Phase Flow

A three-dimensional two-phase flow of a gas containing polydisperse liquid particles is considered. Coagulation, breakage, and rotation of the particles in the flue gas path of an SRM nozzle are taken into account. Every cross section of the path, perpendicular to the nozzle axis, is rectangular. Let us transform the parameters to the dimensionless form as follows:

$$\tilde{\rho} = \rho/\rho_0 \quad \tilde{u} = u/a_* \quad \tilde{v} = v/a_* \quad \tilde{w} = w/a_*$$

$$\tilde{P} = P/P_0 \quad \tilde{T} = T/T_0 \quad \tilde{H}_0 = H_0/RT_0 \quad \tilde{x} = x/r_m$$

$$\tilde{r} = r/r_m \quad \tilde{z} = z/r_m \quad \tilde{y} = y/r_m \quad \tilde{\rho}_i = \rho_i/\rho_0$$

$$\tilde{T}_i = T/T_0 \quad \tilde{u}_i = u_i/a_* \quad \tilde{v}_i = v_i/a_* \quad \tilde{w}_i = w_i/a_*$$

$$\tilde{n}_i = n_i/n_{\text{ref}} \quad \tilde{M}_i = M_i/M_{\text{ref}} \quad \tilde{r}_i = \tilde{r}/r_{\text{ref}}$$

For brevity, the overbars above the dimensionless parameters are omitted. The subsystem of three-dimensional gas-phase equations has the form[2,6]:

$$\frac{\partial E_g}{\partial x} + \frac{\partial F_g}{\partial r} + \frac{\partial G_g}{\partial \theta} + H_g = 0 \qquad (24)$$

where

$$E_g = (\rho u,\ \rho u^2 + \kappa_1 p,\ \rho uv,\ \rho uw,\ \rho u H_0)^T$$

$$F_g = (\rho v,\ \rho uv,\ \rho v^2 + \kappa_1 p,\ \rho vw,\ \rho v H_0)^T$$

$$G_g = (\rho w,\ \rho uw,\ \rho vw,\ \rho w^2 + \kappa_1 p,\ \rho w H_0)^T$$

$$H_g = \begin{Bmatrix} 0 \\ \sum_{i=1}^{N} \rho_i \bar{\varphi}_{Ri}(u - u_i) \\ \sum_{i=1}^{N} \rho_i \bar{\varphi}_{Ri}(v - v_i) \\ \sum_{i=1}^{N} \rho_i \bar{\varphi}_{Ri}(w - w_i) \\ \sum_{i=1}^{N} \rho_i [\bar{\varphi}_{Ai}\kappa(T - T_i)/(\kappa - 1) \\ \quad + \bar{\varphi}_{Ri} U_i (U - U_i)/\kappa_1] \end{Bmatrix}$$

$$\bar{\varphi}_{Ri} = \varphi_{Ri} r_m / a_*, \quad \bar{\varphi}_{Ai} = \varphi_{Ai} r_m / a_*, \quad \kappa_1 = (\kappa + 1)/2\kappa$$

Superscript T denotes transposing a matrix.

The subsystem is closed with the dimensionless state equation

$$p = \rho \frac{\kappa - 1}{\kappa} \left(H_0 - \frac{u^2 + v^2 + w^2}{2\kappa_1} \right) \tag{25}$$

The subsystem of three-dimensional equations for the ith fraction of the particles is written as follows[6,9]:

$$\frac{\partial E_i}{\partial x} + \frac{\partial F_i}{\partial y} + \frac{\partial G_i}{\partial z} + \boldsymbol{H}_i = 0 \tag{26}$$

where

$$E_i = (\rho_i u_i,\ \rho_i u_i^2,\ \rho_i u_i v_i,\ \rho_i u_i w_i,\ \rho_i u_i T_i,\ n_i u_i,\ n_i u_i M_i^2)^T$$

$$F_i = (\rho_i v_i,\ \rho_i u_i v_i,\ \rho_i v_i^2,\ \rho_i v_i w_i,\ \rho_i v_i T_i,\ n_i v_i,\ n_i v_i M_i^2)^T$$

$$G_i = (\rho_i w_i,\ \rho_i u_i w_i,\ \rho_i v_i w_i,\ \rho_i w_i^2,\ \rho_i w_i T_i,\ n_i w_i,\ n_i w_i M_i^2)^T$$

$$H_i = \{-\tilde{Q}_{1i},\ \rho_i \bar{\varphi}_{Ri}(u_i - u) - \tilde{Q}_{2i},\ \rho_i \bar{\varphi}_{Ri}(v_i - v) - \tilde{Q}_{3i},\ \rho_i \bar{\varphi}_{Ri}(w_i - w) - \tilde{Q}_{4i},\ \rho_i \bar{\varphi}_{Ai}(T_i - T)c_p/c_B - \tilde{Q}_{5i},\ -\tilde{Q}_{6i},\ n_i \bar{\varphi}_{Mi} M_i^2 - \tilde{Q}_{7i}\}^T$$

$$\bar{\varphi}_{Mi} = \varphi_{Mi} r_m / a_*, \quad \tilde{Q}_{ji} = Q_{ji} r_m n_{\text{ref}} r_{\text{ref}}^2 \quad (j = 1, 2, \ldots)$$

The coagulation terms Q_{ji} are the same as those in the quasi-one-dimensional case, but with account taken for the spatial components of the velocity vector.

The intervals in which the systems of Eqs. (24) and (26) can be defined are limited by the inlet and outlet sections and the symmetry plane (planes), and differ only in boundary surface. For the gas-phase subsystem, the boundary surface is the real nozzle surface, while the boundary surface for the ith fraction of particles is the so-called "limiting interface," which separates a zone containing the particles of the given fraction and a zone in which such particles are absent.

The numerical calculations are based on the quasiestablishment method.[6,9,31] For more convenient integration of subsystem (24) by the finite difference method, the new independent variables ξ, η, and ζ were obtained by the transformations[32]: $\xi = \xi(x, y, z)$, $\eta = \eta(x, y, z)$, and $\zeta = \zeta(x, y, z)$.

The initial and boundary conditions were chosen as follows. The initial conditions for ρ, u, P, and H_0 were determined on the basis of the quasi-one-dimensional approach. The velocity vector components v and w were obtained by means of linear extrapolation between corresponding values at the boundaries of the calculation region.

Four boundary conditions are set for the nozzle inlet: $H_0(\xi_H, \eta, z) = \text{const}$; $S_0(\xi_H, \eta, \zeta) = \text{const}$; $v(\xi_H, \eta, \zeta)/u(\xi_H, \eta, \zeta) = f_1(\eta, \zeta)$; $w(\xi_H, \eta, \zeta)/u(\xi_H, \eta, \zeta) = f_2(\eta, \zeta)$, with f_1 and f_2 being the given functions. The conditions of impermeability were set for impermeable walls. The conditions of symmetry were specified for the planes $\eta = 0$ and $\zeta = 0$. Because the flow at the nozzle exit section is supersonic, no boundary conditions were set.

The subsystems of Eqs. (26) for particle fractions were integrated along the trajectories of the particles of corresponding fractions. For the solution of these subsystems, all independent parameters of fraction particles at the nozzle exit section were specified. The flow at the exit section was assumed to be equilibrium and, hence, the particle velocities and temperatures were taken as equal to the corresponding gas-phase parameters

$$u_i(\xi_H, \eta, \zeta) = u(\xi_H, \eta, \zeta), \quad v_i(\xi_H, \eta, \zeta) = v(\xi_H, \eta, \zeta)$$

$$w_i(\xi_H, \eta, \zeta) = w(\xi_H, \eta, \zeta), \quad T_i(\xi_H, \eta, \zeta) = T(\xi_H, \eta, \zeta)$$

In addition, the particle-seeded gas densities $\rho_i(\xi_H, \eta, \zeta)$, the number of particles $n_i(\xi_H, \eta, \zeta)$, and the squares of rotational moments M_i^2 were set for the nozzle inlet.

The lines of intersection of nozzle surfaces with the planes $y = 0$ and $z = 0$ were determined by the cosinusoidal–conic dependencies

$$Y(x) = \begin{bmatrix} \dfrac{y_H + y_m}{2} + \dfrac{y_H - y_m}{2} \cos\left(\pi \dfrac{x_H - x}{x_H} \right), & x_H \le x \le x_J \\ y_m + Q_J (x - x_J), & x_J \le x \le x_a \end{bmatrix} \tag{27}$$

where x_H, x_m, x_J, and x_a were the abscissas of the inlet, throat, joint, and exit sections of the nozzle, respectively, with y_H, y_m, and y_J being the profile ordinates for corresponding sections. The dependencies for $Z(x)$ were set in a similar manner. As the calculations were performed for a nozzle with two symmetry planes, the nozzle surface was determined by two functions, $Y_1(x)$ and $Z_1(x)$. The following values of the dimensionless abscissas (referring to the effective throat radius r'_m) were taken: $x_H = 1$, 8, $x_m = 0.0$, $x_J = 0.3$, and $x_a = 0.9$. The values of the ordinates were varied, depending on nozzle geometry. The in-chamber conditions and the parameters of the combustion products of the model propellant composition were as follows: $P_0 = 6.2$ MN/m^2, $T_0 = 3800$ K, $R = 370$ J/kg·K, $\kappa = 1.15$, $z = 0.4$, $\eta_0 = 9 \times 10^{-5}$ kg/(m·s), and $r'_m = 0.03$ m.

The size distribution of particles at the nozzle inlet was set[3] in accordance with the normal logarithmic law with $d_{43} = 5$ μ. The number of particle fractions was eight. Figure 7 shows isometric projections of Mach number isolines and the "limiting interface" projections for the 1, 3, 5, and 8 fractions in a SRM nozzle with a rectangular inlet section with the coordinates $y_H = 1.8$ and $z_H = 1.4$, and a square throat with the coordinates $y_m = z_m = 1$.

It should be noted that the flow is essentially three dimensional. The Mach number isolines in the longitudinal and cross sections, and particularly near the nozzle walls, are nonuniform. The isolines show considerable inflections at the limiting interface of particle fractions. In addition, the isolines in the $z = 0$ plane are more bent than those in the $y = 0$ plane. This is associated with the lesser curvature of the wall $Z(x)$ in the subsonic region. At the joints of the cosinusoidal and

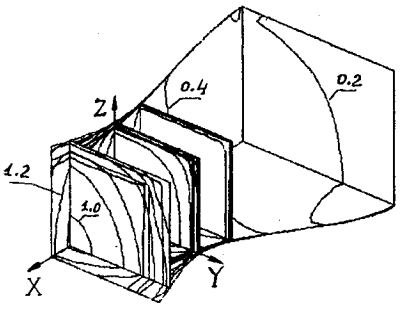

Fig. 7 Isometric projections of the Mach number isolines and limiting interfaces.

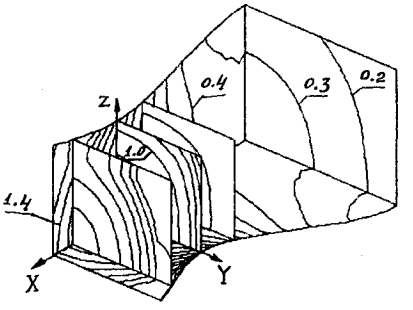

Fig. 8 Isometric projections of the Mach numbers for an equilibrium flow.

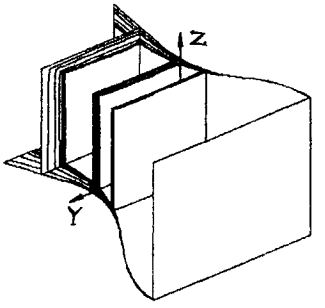

Fig. 9 Limiting interfaces of particle fractions.

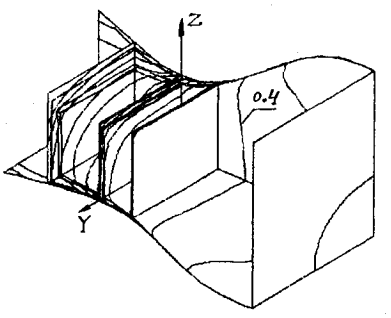

Fig. 10 Isometric projections of the Mach numbers for a rectangular throat.

conic sections, where the second spatial derivatives are disrupted, shock waves are formed. For comparison, the calculation of an equilibrium (with equal gas and particle velocities) two-phase flow was performed for the same nozzle (Fig. 8). A comparison of the Mach number isolines in Figs. 7 and 8 reveals certain differences in the flow patterns. The sonic surface for the equilibrium flow is closest to the throat, and it is shifted to the divergent section up to $x \approx 0.65 \times r'_m$ for the two-phase flow. The corresponding isolines in the last cross sections in the figures indicate that the Mach numbers for the equilibrium flow are higher and that the supersonic flow pattern begins near the nozzle walls. In the case of the two-phase flow, transformation to the supersonic flow starts later. The three-dimensional character of the flow is readily distinguished by the positions of the limiting interfaces of the particles of different fractions shown in Fig. 9. The stratification of the limiting interfaces is rather significant, and depends on the steepness of the nozzle surface in the subsonic region. It can be readily seen in Fig. 9 that the departure of particle paths from wall Y is larger than that from wall Z. Also of interest are the positions of the limiting interfaces in the nozzle cross sections. Different values of the departure from the lateral walls lead to deformation of the limiting interfaces. The same situation can be seen in Fig. 10, which shows a nozzle with a square inlet section ($y_H = z_H = 1.5$) and a rectangular throat ($y_m = 1.0$, $z_m = 0.7$). It should also be noted that for this nozzle the Mach number isolines in the cross section are elliptic, while the cross section of corresponding lines in Fig. 7 is close to a circle; this supports the well-known fact that the supersonic flow is formed mainly in the transonic section of the nozzle.

Axisymmetric Flow with Intersection of Trajectories of Particles

Figure 11 shows a simple charge of propellant with a ring slot extending the burning surface. The crossing main flow and the flow from the slot form a mixing zone in the channel, wherein particles of the same size have different velocities and temperatures. The size distribution of particles changes is essentially due to their coagulation and breaking in this zone. To derive a system of equations for the description of particle behavior in this case, it is reasonable to study the evolution of groups of particles with close parameters at the boundary of the calculation region. Let us divide all particles ejected from the charge into separate characteristic flows in order to avoid ambiguous solutions in calculations for each characteristic flow. The flows are denoted by the letters α and β. The continuous size distribution of particles in each flow is changed for a finite number of particle fractions. The particles of the fraction s from flow number α are referred to as (s, α) particles.

The formulation of mathematical models for such groups of particles is rather difficult, since on collisions followed by coagulation or breaking, liquid particles lose the characteristics typical of the initial particle groups. To circumvent this problem, we assume that the parameters of all colliding particles change continuously and at the same velocity. This approach investigating collision-induced changes in the parameters of polydisperse droplets without considering possible temperature and velocity differences of particles of the same fractions has been proposed by Sternin et al.[5] It is based on considering the statistical average of mass variations of target particles affected by missile particles. The mass of each missile particle is less than the mass of the corresponding target particle. The change in mass of the (s, α) target particles at a large number A of collisions with the (l, β) particles is calculated by the equation

$$Adm_s^\alpha = A\phi_{sl}^{\alpha\beta} m_l^\beta \tag{28}$$

where m_l^β is the mass of the (l, β) missile particles, and $\phi_{sl}^{\alpha\beta}$

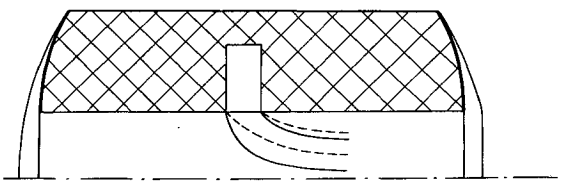

Fig. 11 Intersection of particle flows in a charge channel.

is the statistical average of the dimensionless fraction of the mass of a missile particle joining a target particle upon collision. The value of $\phi_{sl}^{\alpha\beta}$ is determined using the dependence form given in Ref. 6. In doing so, it is assumed that the total mass joining the targets is uniformly distributed over all particles. For simplicity, we also assume that the mass exchange between missiles and targets occurs only because of the changed number of missiles, with the individual missile masses remaining unchanged. The numbers of particle fractions are ordered so that for every a at the initial points of each particle trajectory, the masses of particles of different fractions meet the condition $m_{sl}^{\alpha} > m_{s2}^{\alpha}$ at $s_2 > s_l$. Let n_s^{α} be the number of (s, α) particles, and n_l^{β} be the number of (l, β) particles per unit volume of mixture. Then the number of collisions of the (s, α) and (l, β) particles per unit volume per unit time is $k_{sl}^{\alpha\beta} n_s^{\alpha} n_l^{\beta}$.

According to Eq. (28), these collisions change the mass of the large (s, α) particles by the value

$$K_{sl}^{\alpha\beta} n_s^{\alpha} n_l^{\beta} \phi_{sl}^{\alpha\beta} m_l^{\beta}$$

and all collisions of such particles with smaller ones change the mass of the (s, α) particles by the value

$$n_s^{\alpha} \frac{\mathrm{d}m_s^{\alpha}}{\mathrm{d}t} = \sum_{\beta} \sum_{l=1}^{l(\beta)} K_{sl}^{\alpha\beta} \phi_{sl}^{\alpha\beta} m_l^{\beta} n_l^{\beta} n_s^{\alpha} \tag{29}$$

The sum in Eq. (8) is calculated for all flows β crossing the local area under consideration, and the numbers $l(\beta)$ are chosen so that the inequalities $\max m_l^{\beta} < m_s^{\alpha}$ are met [at equal masses the value under the summation sign is added to the group (s, α) if $\alpha < \beta$].

On calculating the change in the number of particles according to the above assumptions, we taken into account only the collisions of the (s, a) particles with large particles. The number of the (s, a) particles joining large particles per unit time and unit volume, including Eq. (28), is

$$\sum_{\beta} \sum_{l=l_1(\beta)}^{N^{\beta}} \frac{K_{sl}^{\alpha\beta} \phi_{sl}^{\alpha\beta} m_l^{\beta} n_l^{\beta} n_s^{\alpha}}{m_l^{\beta}} \tag{30}$$

where the number $l_1(\beta)$ is chosen such that $\min m_l^{\beta} > m_s^{\alpha}$ (at equal masses, the corresponding term in the sum is taken into account only if $\alpha > \beta$).

With account of Eq. (30), the equation of conservation of number for the (s, α) particles is written in the form

$$\frac{\partial n_s^{\alpha}}{\partial t} + \nabla \cdot (\boldsymbol{U}_s^{\alpha} n_s^{\alpha}) = -\sum_{\beta} \sum_{l=l_1(\beta)}^{N^{\beta}} K_{sl}^{\alpha\beta} \phi_{sl}^{\alpha\beta} n_s^{\alpha} n_l^{\beta} \tag{31}$$

In deriving the equations of momentum of particles in terms of the proposed model, it is assumed that every missile particle joined to a fraction of larger particles brings its momentum to this fraction. According to experimental works on modeling particle collisions in SRM, the postcollision velocities of particle fragments are close in magnitude.[3,4] Therefore, the missile particles that do not join larger particles in collisions are assumed to remain in the group having the velocity of target particles.

Thus, all particles from particle groups of less masses, colliding with the (s, α) particles bring to the (s, α) group the momentum

$$\sum_{\beta} \sum_{l=1}^{l(\beta)} K_{sl}^{\alpha\beta} n_s^{\alpha} n_l^{\beta} \boldsymbol{U}_l^{\beta} m_l^{\beta}$$

while the fragments returning to the initial fraction carry away from the (s, α) group the momentum

$$\sum_{\beta} \sum_{l=1}^{l(\beta)} K_{sl}^{\alpha\beta} (1 - \phi_{sl}^{\alpha\beta}) n_s^{\alpha} n_l^{\beta} m_l^{\beta} \boldsymbol{U}_s^{\alpha}$$

The particles of the (s, a) group colliding with larger particles carry away from the (s, a) group the momentum

$$\sum_{\beta} \sum_{l=l_1(\beta)}^{N^{\beta}} K_{sl}^{\alpha\beta} n_s^{\alpha} n_l^{\beta} m_s^{\alpha} \boldsymbol{U}_s^{\alpha}$$

At the same time, the particles that do not join larger particles in collisions go back to their initial group, bringing there the momentum

$$\sum_{\beta} \sum_{l=l_1(\beta)}^{N^{\beta}} K_{sl}^{\alpha\beta} (1 - \phi_{sl}^{\alpha\beta}) n_s^{\alpha} n_l^{\beta} m_s^{\alpha} \boldsymbol{U}_l^{\beta}$$

Taking into account the change in the momentum of particles caused by their interaction with gas due to the drag force F_s^{α}, we write the equation of conservation of momentum for the (s, α) particles as

$$\begin{aligned} \frac{\partial}{\partial t} (m_s^{\alpha} n_s^{\alpha} u_{sk}^{\alpha}) + \nabla \cdot (m_s^{\alpha} n_s^{\alpha} u_{sk}^{\alpha} \boldsymbol{U}_s^{\alpha}) &= \sum_{\beta} \sum_{l=1}^{l(\beta)} K_{sl}^{\alpha\beta} n_s^{\alpha} n_l^{\beta} m_l^{\beta} u_{lk}^{\beta} \\ &- \sum_{\beta} \sum_{l=1}^{l(\beta)} K_{sl}^{\alpha\beta} (1 - \phi_{sl}^{\alpha\beta}) n_s^{\alpha} n_l^{\beta} m_l^{\beta} u_{sk}^{\alpha} \\ &- \sum_{\beta} \sum_{l_1(\beta)}^{N^{\beta}} K_{sl}^{\alpha\beta} n_s^{\alpha} n_l^{\beta} m_s^{\alpha} u_{sk}^{\alpha} \\ &+ \sum_{\beta} \sum_{l_1(\beta)}^{N^{\beta}} K_{sl}^{\alpha\beta} (1 - \phi_{sl}^{\alpha\beta}) n_s^{\alpha} n_l^{\beta} m_s^{\alpha} u_{lk}^{\beta} + n_s^{\alpha} F_{sk}^{\alpha} \end{aligned} \tag{32}$$

Assuming that the temperatures of particles in collisions have sufficient time to reach an equilibrium (as do velocities), and using reasoning similar to that employed in deriving the equations for momentum, one can write an equation for the particle temperature T_s^{α}, which must be solved in combination with the gas-phase equations.

The discussed model was used to investigate a stationary axisymmetric flow in a cylindrical channel with a ring-shaped slot (Fig. 11). The channel was 2.2 m in length and 0.25 m in diameter. The width of the ring was equal to the channel radius. The flow rate of combustion products from the ring slot was 20% total mass supply. Three channel modifications with different distances between the ring slot and the head-end of the motor (0.3, 1.1, and 2.05 m) were considered. The pressure at the channel outlet was 6 MPa. The dimensionless mass concentration of particles in the flow was taken equal to 0.4. The initial size distribution of particles was calculated by the normal logarithmic law, with the mass mean diameter 2 μ. The two-phase flow at the efflux surfaces was considered equilibrium. The gas-phase parameters were calculated by the stabilization method.

Figure 12 shows a calculated change in mass mean size of particles along the channel axis for the case in which the ring slot is in the center of the channel. The blow-in region, characterized by strong particle coagulation leading to increasing size of particles, is due to the crossing of different particle flows and the nonuniformity of the general flow.

Figure 13 shows calculation results for local mass mean sizes of particles at different distances from the channel axis at the channel outlet section. Curve 1 is the dependence for the ring slot located at the beginning of the channel. Curve 2 is the dependence calculated for the centered slot. Curve 3 corresponds to the situation in which the slot is placed near the channel exit section.

The calculation results also show that the maximum particle sizes are observed in the case in which an additional flow is injected in the beginning of the channel and the interaction time is maximum. Coagulation in this situation is favored by the increased concentration of particles near the channel axis due to the high velocity of the injected flow.

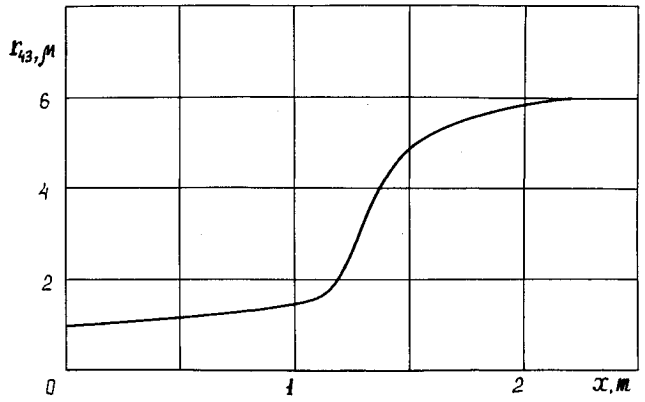

Fig. 12 Change in mass mean radius of particles along a channel with a ring-shaped slot at the center.

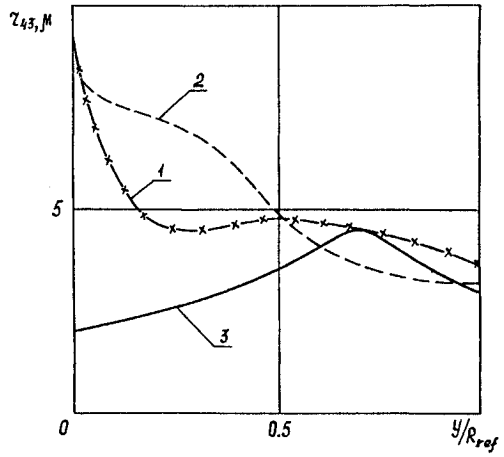

Fig. 13 Profiles of mass mean particle radius at the nozzle inlet section for different slot positions along the charge channel (1, head end; 2, central part; and 3, exit end).

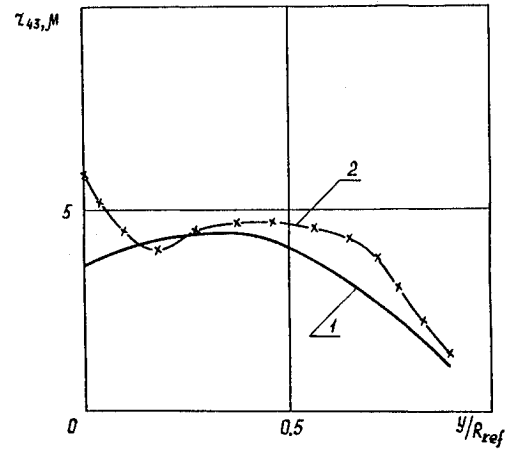

Fig. 14 Profiles of mass mean particle radius at the nozzle outlet section for channels with a slot in the exit end (curve 1) and in the head end (curve 2).

However, the great difference in particles sizes in the cases considered has an insignificant effect on SRM performance. The calculation performed by the technique[6] taking into account coagulation, breakage, and rotation of particles in axisymmetric nozzles of SRM shows that the specific impulse to change is only 0.5%. This is accounted for by the breakage of large particles by the gas flow in the nozzle throat. Figure 14 presents axisymmetric profiles of mass mean sizes of particles in the exit nozzle section for charge configurations with a slot at the end and at the beginning of the charge. It can be seen that the particle sizes at the nozzle exit section differ insignificantly.

Conclusions

The results of numerical calculations of a quasi-one-dimensional two-phase flow, taking into account particle coagulation, breakage, and rotation, have shown that these processes produce a complex effect on the magnitude of the two-phase losses.

Three-dimensional calculations for nozzles of rectangular cross sections point to the essentially three-dimensional pattern of the two-phase flow, which differs from that for pure gas flow.

An approach has been proposed that allows application of the multiple-liquid model to calculating two-phase flows, including the crossing of the paths of particles of the same size. It has been shown that path crossing affects the size distribution of condensed particles.

References

[1]Alemasov, V. E., Dregalin, A. F., Tishin, A. P., Hudyakov, V. A., and Glushko, V. P. (eds.), *Thermodynamic and Thermophysical Properties of Combustion Products*, Vol. 1, VINITI AN SSSR, Moscow, 1971. Translated into English from Russian, by Kerer Press, Jerusalem, 1974.

[2]Kraiko, A. N., Nigmatulin, R. I., Starkov, V. K., and Sternin, L. E., "Mechanics of Multi-Phase Media," *Hydromechanics*, Vol. 6, VINITI AN SSSR, Moscow, 1972, pp. 93–174.

[3]Sternin, L. E., *Foundations of Gas Dynamics of Two-Phase Flows in Nozzles*, Mashinostroenie, Moscow, 1974.

[4]Pirumov, U. G., and Roslyakov, G. S., *Gas Flow of Nozzles*, Springer–Verlag, Berlin, 1986.

[5]Sternin, L. E., Maslov, B. N., Shraiber, A. A., and Podvysotskii, A. M., *Two-Phase Mono- and Polydisperse Gas-Particle Flows*, Mashinostroenie, Moscow, 1980.

[6]Vasenin, I. M., Arkhipov, V. A., Butov, V. G., Glazunov, A. A., and Trofimov, V. F., *Gas Dynamics of Two-Phase Flows in Nozzles*, Tomsk State Univ. Press, Tomsk, Russia, 1986.

[7]Yanenko, N. N., Soloukhin, R. I., Papyrin, A. N., and Fomin, V. M., *Supersonic Two-Phase Flows Under Nonequilibrium of the Particle Velocities*, Nauka, Novosibirsk, Russia, 1980.

[8]Shraiber, A. A., "Multi-Phase Polydisperse Flows with Variable Fraction Composition of Discrete Inclusions," *Itogi Nauki i Tekhniki*, Vol. 3, 1988, pp. 3–80.

[9]Rychkov, A. D., *Mathematical Modeling of Gas Dynamic Processes in Channels and Nozzles*, Nauka, Novosibirsk, Russia, 1988, p. 223.

[10]Nigmatulin, R. I., *Dynamics of Multi-Phase Media, Part I*, Nauka, Moscow, 1987, pp. 1–464.

[11]Deich, M. E., and Filippov, G. A., *Two-Phase Flows in Heat Power Industry Units*, Energoatomizdat, Moscow, 1987, pp. 1–328.

[12]Grishin, S. D., Tishin, A. P., and Khairutdinov, R. I., "Non-Equilibrium Two-Phase Flows in de Laval Nozzles, Including the Coagulation of Condensed Particles," *Izvestiya AN SSSR, Mekhanika Zhidkosti i Gaza*, No. 2, 1969, pp. 112–117.

[13]Tishin, A. P., and Khairutdinov, R. I., "Calculation of Condensed Particle Coagulation in de Laval Nozzles," *Izvestiya AN SSSR, Mekhaaanika Zhidkosti i Gaza*, No. 5, 1971, pp. 181–185.

[14]Crowe, C. T., and Willoughby, P. G., "A Mechanism for Particle Growth in a Rocket Nozzle," *AIAA Journal*, Vol. 4, No. 9, 1966, pp. 1677–1679.

[15]Crowe, C. T., and Willoughby, P. G., "A Study of Particle Growth in a Rocket Nozzle," *AIAA Journal*, Vol. 5, No. 7, 1967, pp. 1300–1304.

[16]Babukha, G. L., Sternin, L. E., and Shraiber, A. A., "Calculation of Two-Phase Losses in Nozzles with Coagulation and Fragmentation of Condensed Droplets," *Izvestiya AN SSSR, Mekhanika Zhidkosti i Gaza*, No. 1, 1971, pp. 175–177.

[17]Podvysotskii, A. M., and Shraiber, A. A., "Calculation of a Non-Equilibrium Two-Phase Flow with Coagulation and Fragmentation of Condensed Particles for an Arbitrary Distribution of Secondary Droplets in Mass and Velocity," *Izvestiga AN SSSR, Mekhanika*

Zhidkosti i Gaza, No. 2, 1975, pp. 71–79.

[18]Rychkov, A. D., and Tkachenko, A. S., "Numerical Study of Supersonic Spatial Two-Phase Flows in Movable Nozzles," *Gazodinamika Mnogofaznykh Potokov v Energoustanovkakh*, Vol. 1, Khar'kov Aviation Inst. Press, Khar'kov, Ukraine, 1978, pp. 8–13.

[19]Chang, I-S., "Three-Dimensional, Two-Phase Supersonic Nozzle Flows," *AIAA Journal*, Vol. 21, No. 5, 1983, pp. 671–678.

[20]Dash, S. M., and Del Guidice, P. D., "Three-Dimensional Ducted and Exhaust Plume Flow Fields," *AIAA Journal*, Vol. 16, 1978, pp. 823–830.

[21]Tkachenko, A. S., "Numerical Modeling of Thrust Characteristics and Structure of Spatial Flows in Nozzles," *Izvestiya AN SSSR, Mekhanika Zhidkosti i Gaza*, No. 5, 1981, pp. 168–173.

[22]Gilinskii, M. M., and Simanovskii, G. P., "Three-Dimensional Two-Phase Gas-Particles Flow in de Laval Nozzle," *Struinye i Otryvnye Techeniya*, Moscow Univ. Press, Moscow, 1979, pp. 51–56.

[23]Gilinskiki, M. M., Stasenko, A. L., and Shuinov, A. V., "Three-Dimensional Two-Phase Flow of a Monodisperse Mixture in de Laval Nozzle," *Struinye i Otryvnye Techeniya*, Moscow Univ. Press, Moscow, 1981, pp. 84–90.

[24]Glazunov, A. A., and Shpigunov, S. V., "Spatial Supersonic Polydisperse Flows in Nozzles with Rectangular Cross-Sections," *All-Union Conference on Application of Powder Technology Apparatus in National Economy*, Book of Abstracts, Tomsk State Univ., Tomsk, Russia, 1987, pp. 225, 226.

[25]Glazunov, A. A., Kuvshinov, N. E., and Shigunov, S. V., "Three-Dimensional Two-Phase Flows in Nozzles with Rectangular Cross-Sections," *Makroskopicheskaya Kinetika i Khimicheskaya Gaazodinamika*, Tomsk, Russia, 1989, pp. 22–25.

[26]Butov, V. G., Vasenin, I. M., and Dyachenko, N. N., "A Model for Motion of Polydisperse Condensate with Regard to Random Pulsations of Velocity and Temperature of Coagulating Particles," *Izvestiya AN SSSR, Mekhanika Zhidkosti i Gaza*, No. 3, 1981, pp. 33–39.

[27]Vasenin, I. M., Arkhipov, V. A., Glazunov, A. A., and Trofimov, V. F., "A Study of Polydisperse Flow in Nozzles with Regard to Particle Rotation," *Inzhenerno-Fizicheskii Sbornik*, Tomsk, Russia, 1985, pp. 31–35.

[28]Henderson, C. B., "Drag Coefficients of Spheres in Continuum and Rarefied Flows," *AIAA Journal*, Vol. 14, 1976, pp. 707, 708.

[29]Carlson, D. J., and Hoglund, R. F., "Particle Drag and Heat Transfer in Rocket Nozzles," *AIAA Journal*, Vol. 2, No. 11, 1964, pp. 1980–1984.

[30]Kisarov, Yu. F., and Lipanov, A. M., "Calculation of the Parameters of a Two-Phase Flow in Axisymmetric de Laval Nozzle with Regard to the Coagulation and Fragmentation of Particles," *Izvestiya AN SSSR, Mekhanika Zhidkosti i Gaza*, No. 4, 1975, pp. 42–46.

[31]Vasenin, I. M., Glazunov, A. A., and Ivanov, V. A., "Numerical Modeling of Two-Phase Flows in Plug Nozzles," *Izvestiya Vysshikh Uchebnykh Zavedenii, Fizika*, No. 8, Tomsk Univ. Press, Tomsk, Russia, 1993, pp. 81–91.

[32]Vasenin, I. M., Glazunov, A. A., Kuvshinov, N. E., Narimanov, R. K., Ivanov, V. A., Shpigunov, S. W., "Modeling of Two Phase Flows in Channels and Nozzles," *Izvestiya Vysshikh Uchebnykh Zavedenii, Fizika*, No. 8, Tomsk Univ. Press, Tomsk, Russia, 1992, pp. 71–81.